Evidence of advective heating by hot fluids of an Alpine fissure in Lauzière Granite (Belledonne massif, Western Alps)

Emilie Janots[1, 2], Alexis Grand'Homme[1], Matthias Bernet[1], Damien Guillaume[3], Edwin Gnos[4], Marie-Christine Boiron[5], Magali Rossi[6], Anne-Magali Seydoux-Guillaume[3], Roger De Ascenção Guedes[7]

[1] Univ. Grenoble Alpes, CNRS, IRD, IFSTTAR, ISTerre, 38000 Grenoble, France
[2] Department of Earth and Environmental Sciences, Ludwig-Maximilians-Universität Munich, Luisenstr, 37, 80333 Munich, Germany
[3] Univ Lyon, UJM-Saint-Etienne, UCA, CNRS, IRD, LMV UMR 6524, F-42023, SAINT-ETIENNE, France.
[4] Natural History Museum of Geneva, 1 route de Malagnou, CH-1208 Geneva
[5] Université de Lorraine, CNRS, GeoRessources, F- 54000 Nancy, France
[6] Univ. Grenoble Alpes, Univ. Savoie Mont-Blanc, CNRS, EDYTEM, 73 000 Chambéry
[7] Editions du Piat, Glavenas, F-43200 Saint-Julien-du-Pinet, France

Correspondence to: Emilie Janots (emilie.janots@univ-grenoble-alpes.fr)

Abstract. A multi-method approach investigation in the Lauzière granite, located in the external Belledonne massif of the French Alps, reveals unusually hot hydrothermal conditions in vertical open fractures (Alpine-type clefts), caused by advective heating. The host-rock granite shows sub-vertical mylonitic microstructures and partial retrogression at temperatures of <400°C during Alpine tectonometamorphism. Novel zircon fission-track (ZFT) data in the granite give ages at 16.3 ± 1.9 and 14.3 ± 1.6 Ma, confirming that Alpine metamorphism was high enough to reset the pre-alpine cooling ages and that the Lauzière granite had already cooled below <240-280°C and was exhumed to <10 km at that time. Novel microthermometric data and chemical compositions of fluid inclusions obtained on millimetric monazite and on quartz crystals from the same cleft indicate early precipitation of monazite from a hot fluid at T>410°C, followed by a main stage of quartz growth at 300-320°C and 1.5-2.2 kbar. Previous Th-Pb dating of cleft monazite at 12.4 ± 0.1 Ma clearly indicates that this hot fluid infiltration took place significantly later than the peak of the Alpine metamorphism. Advective heating due to the hot fluid flow caused resetting of fission-tracks in zircon in the cleft hanging wall, with a ZFT age at 10.3 ± 1.0 Ma. The results attest of highly dynamic fluid pathways, allowing the circulation of deep mid-crustal fluids, 150-250°C hotter than

the host-rock, which affect the thermal regime only at the wall-rock of the Alpine-type cleft. Such advective heating may impact the ZFT data and represent a pitfall for exhumation rate reconstructions in areas affected by hydrothermal fluid flow.

1 Introduction

Geochronological datasets in external parts of mountain belts are primordial to date metamorphism, deformation and fluid activity, to model exhumation rates, and to assess the role of tectonic activity, topography and climate influence on orogenic evolution. Geochronological data can either be interpreted as apparent cooling ages or crystallisation ages. Apparent cooling ages are assumed to record the time at which a rock cooled below the closure temperature of the thermochronometer (Reiners and Brandon, 2006). Exhumation rates can thus be derived by correlating the apparent cooling ages with the closure depth for a given geothermal gradient (Brandon et al., 1998; Willet and Brandon, 2013). For geochronometers with closure temperatures above the rock/mineral (re)-crystallization temperature, geochronological data record the age of crystallisation. Petrochronology is an emerging field of Earth Sciences aiming to characterize the crystallisation conditions associated with ages based on petrological characterisations (Engi et al., 2017). Combining thermochonological data with crystallisation ages is powerful to evaluate the possibility of increased tectonic or fluid activity, which can affect the estimation of exhumation rates.

Crystallisation during exhumation (retrogression) is commonly related to deformation and fluid circulation, because retrogression involves hydration reactions and mass transfer requires fluid (e.g., Austrheim and Griffin, 1985; Putnis and Austrheim, 2010). This is particularly true for basement rocks in external parts of orogenic belts, where crystalline rocks mainly made of anhydrous minerals are submitted to low-temperature retrogression, which are slowing down mineral reaction kinetics. For example in the external crystalline massifs (ECM) of the Alps, retrogression occurs at temperatures <400°C and is commonly localized in highly deformed domains (e.g. shear zone, mylonite; Bellanger et al., 2015; Rossi et al., 2005) with evidence of fluid circulation causing vein formation, metasomatism, or fluid assisted reactions (Rossi and Rolland, 2014). Ascending fluids can also modify the temperature gradient by advective heating, but the influence of fluid flow on thermochronological data is rarely considered in exhumation reconstructions (Derry et al., 2009; Whipp and Ehlers, 2007), and remains to be quantified through numerical modelling.

In natural environments, the age and impact of hydrothermal activity on the thermal structure is difficult to quantify because it requires evaluating the fluid flux in a system that is partially open and multistage. New insights have recently been gained from in-situ monazite-(Ce) (hereafter called monazite) dating in hydrothermal clefts (open fissures partly filled by hydrothermally grown minerals). This provides precise constraints on the timing, duration and periodicity of hydrothermal precipitation during late-stage deformation (Bergemann et al., 2017; Berger et al., 2013; Janots et al., 2012). In the ECM, the crystallization ages of cleft monazite fall generally within the relatively large range of zircon fission-track (ZFT) ages (Berger et al., 2013; Gnos et al., 2015; Grand'Homme et al., 2016), which vary depending on the massifs and structural

positions. The meaning of this age overlap is currently questioned.in terms of possible feedbacks between fluid flow and cooling during exhumation, and resetting of the ZFT thermochronometer in presence of hot fluids (Grand'Homme et al., 2016). First, an age overlap may indicate that monazite precipitated when the fluid cooled below the ZFT closure temperature (Gnos et al., 2015), due to exhumation of the cleft and its surrounding host-rock. This is however contradictory with the short-duration and episodic growth of cleft monazite (Janots et al., 2012) suggesting that it precipitates due to tectonic/hydrothermal activity rather than by progressive cooling during exhumation (Bergmann et al., 2017; Gasquet et al., 2010; Grand'Homme et al., 2016). Second, it may indicate that host-rock fracturing and fluid flow causing monazite growth occurred when the temperature of the host-rock was close to the ZFT closure temperature. Finally, the overlap of the cleft monazite age with ZFT data could indicate advective heating by fluids that were hotter than the closure temperature of the ZFT thermochronometer, leading to partial resetting of the ZFT age until the thermal effect of the fluid on the host-rock ceases. To resolve this question requires to determine the temperature of the fluids that penetrate the cleft and to evaluate its thermal impact on the host-rock.

In this paper, novel LA-ICP-MS and microthermometric data on fluid inclusions in monazite and quartz were obtained to successfully determine the temperature of mineral precipitations in a fissure system (cleft) that formed during exhumation of the Lauzière Granite (Belledonne massif, Western Alps). Combined with the age of the monazite crystals previously dated by Grand'homme et al. (2016), microthermometric data in monazite reveal the circulation of fluids significantly hotter than the host-rock. The impact of the advective heating on the thermal regime of the host-rock appears however local, as evaluated from ZFT data in host rock granite samples collected at the direct contact, 30 meters and 100 meters away from the cleft.

2 Geological Settings and samples

The Alpine belt results from the closure of the Tethys Ocean and the subsequent collision between the Eurasian and Adriatic plates. The investigated outcrop is located in the Lauzière granite (Fig. 1; 45°28'52.90"N; 6°23'6.18"E), in the northern prolongation of the Belledonne massif, which belongs to the external crystalline massifs (ECM; Fig. 1a). The ECM consist of blocks of Variscan basement of the European margin. They correspond to the westernmost paleogeographic units and are distinguished from the Internal domains, consisting of more distal paleogeographic units that underwent higher grade metamorphic overprinting during the Alpine subduction-collision cycle. The ECM were thrust under the internal domains following the activation of the Penninic front during Oligocene-Miocene times (Dumont et al., 2008). Related metamorphism was never evaluated in the Lauzière granite, and remains poorly constrained in the Belledonne massif (320°C-350°C; Nziengui, 1993). It is assumed to lie between the metamorphic conditions of the Mont Blanc massif in the north (400°C, <5 kbar; Rolland et al., 2003; Rossi et al., 2005) and the Oisans massif to the south (270-360°C, 2-5 kbar; review in Bellanger et al., 2015). A complex geochronological dataset exists for the metamorphism recorded in shear zones and veins in the ECM, with three age-groups at ca. 24-30 Ma; 20-12 Ma and 12-6 Ma, attributed to the different deformation

stages (Gasquet et al., 2010; Leloup et al., 2005; Rolland and Rossi, 2016). Underthrusting of the ECM is generally estimated to have occurred around 30 Ma (Bellanger et al., 2015; Cenki-Tok et al., 2011; Nziengui, 1993; Rolland and Rossi, 2016). The Ar–Ar and ZFT datasets suggest that cooling and exhumation started at ca. 18 Ma (Boutoux et al., 2016; Seward and Mancktelow, 1994), in a compressive tectonic regime until 12 Ma (dating in horizontal veins; Bergemann et al., 2017; Gasquet et al., 2010; Rossi and Rolland, 2014). Finally, a transpressive regime (dextral strike slip) prevailed at 12-10 and 6-8 Ma. This has been constrained through in-situ U-Th-Pb dating of monazite crystals collected in vertical fissures (Bergemann et al., 2017; Gasquet et al., 2010; Grand'Homme et al., 2016).

Samples of the Lauzière granite were collected below the "Entre deux roches" pass (Fig. 2a), which is located at the south-eastern margin of the Lauzière massif, 2 km westward from the major Ornon-Roselend fault separating the ECM from Mesozoic sedimentary formations (Fig. 1b). The Lauzière granite is a late-Variscan complex dated at 341 ± 13 Ma (Debon et al., 1998). In the investigated outcrop, the deformation is pervasive (mylonite) with N020-040 oriented subvertical foliation. Despite of variable strain and retrogression, the original K-feldspar-albite-quartz-biotite assemblage of the monzogranite is readily identified microscopically by ubiquitous mm-sized titanite pseudomorphoses (leucoxene). Retrogression is characterized by biotite and K-feldspar breakdown as well as growth of fine-grained albite and low-temperature white mica. In this outcrop, efficient fluid circulation with relatively high fluid/rock ratio is evidenced by the pervasive retrogression in the mylonite similar to that described by Rolland and Rossi (2016) in the Mont Blanc massif, and by the presence of subvertical veins that are typically cm-sized. The investigated Alpine-cleft (Fig. 2b) is a several meters sized cavity partly filled by hydrothermally grown minerals. This cleft is subvertical and oriented perpendicular to the main host-rock foliation (N110; Grand'Homme et al., 2016). At the cleft contact, the host-rock shows strong alteration with abundant white mica (biotite-free).

Five granitic samples were collected at similar altitude along a ~100 m profile (Fig. 2a). Sample collection strategy was aimed to compare the ZFT age obtained at the cleft contact (sample R1) to ages of host-rock samples that remained unaffected by significant late-stage fluid (samples R2 and R3 at 30 m and 100 m of the cleft, respectively). The host-rock samples were taken in areas devoid of veins in their direct vicinity. At the cleft contact, the granite has a smaller grain size (higher strain) and higher abundance of white mica (higher retrogression) compared to host-rock samples taken further away from the cleft. Of the five host-rock samples prepared for zircon fission track analyses, only 3 provided successful results.

Additional samples were collected within the cleft (Fig. 2c). They consist of mm- to cm-sized quartz (, albite, adularia, chlorite and also accessory minerals such as anatase, rutile, ilmenite, apatite, monazite, xenotime, and rare sulfosalts as meneghinite (Moëlo et al., 2002). The cleft contains abundant millimetric monazite grains (prisms up to 9 mm), which were previously dated in-situ using LA-ICP-MS (Grand'Homme et al., 2016). Although the monazite grains were zoned, Th-Pb ages (12.4 ± 0.1 Ma; MSWD = 1.7) and U-Pb ages (12.2 ± 0.2 Ma; MSWD = 1.1) are concordant, with overlap of ages obtained on different grains and in different compositional domains within a grain. This U-Th-Pb dating indicates a short-duration growth of hydrothermal monazite. Furthermore, these monazite crystals contain fluid inclusions, offering the possibility to correlate crystallization age with the physicochemical conditions of the hydrothermal episode.

Amongst the 15 hand-specimen containing mm-sized monazite, we separated associations of contiguous monazite and quartz crystals (samples E2R2, E2R3, E2R4) and adjacent quartz crystals (samples E2R1, E2R31). Most quartz crystals are mm-sized, but the E2R3 (-a, -b, -c) and E2R31 (-a, -b) are fragments from cm-sized crystals. When monazite and quartz were found contiguous, quartz seems to lie over monazite and thus to have grown after it.

3 Methods

3.1 Fluid inclusions analysis

Microthermometric measurements were performed with a Linkam THMS600 heating-freezing stage mounted on a BX-51 Olympus microscope at the Geosciences Environnement Toulouse (GET) laboratory and the GeoRessources laboratory (Nancy). Temperatures of the following phase changes were measured: eutectic melting (T_e), ice melting (T_m ice), and total homogenization (T_h). According to the calibration curves and the type of phase changes, temperatures are given with an accuracy of about ± 5°C for T_e, and ± 0.2°C for T_m ice and T_h. Fluid composition analyses of inclusions in quartz were carried out by LA-ICP-MS analyses at the GeoRessources laboratory (Nancy, France) following protocols published in Leisen et al. (2012). The LA-ICP-MS system is composed of a GeoLas excimer laser (ArF, 193nm, Microlas, Göttingen, Germany), with a microscope for sample observation and laser beam focus onto the sample and an Agilent 7500c quadrupole ICP-MS. The sample is located inside a cylindrical ablation cell, attached to a motorized X-Y stage of an optical microscope (® Olympus BX-41). The laser beam is focused onto the sample with a Schwarztschild reflective objective (magnification X 25). The ablated material is carried in helium gas, which is mixed with argon via a cyclone mixer prior to entering the ICP torch, following the procedures outlined by Roedder (1984) and Sheperd et al. (1985). Quartz and monazite individual crystals were double-polished, and ~200 to 300-µm-thick sections were prepared for fluid inclusion studies (Figs. 3a and 3b).

3.2 Zircon fission tracks

In sample R1 (cleft contact), the smaller grain size (higher strain) resulted in a low zircon yield. Because many zircons were fractured, had strong uranium zoning and/or inclusions, only 7 zircons could be extracted from sample R1, compared to up to 12 zircons in the other samples (R2 and R3). Zircon grains were mounted in Teflon® sheets, polished and etched at 228°C for 16-40 hours in a NaOH-KOH melt. Using the external detector method, all samples were irradiated together with IRMM541 dosimeter glasses and Fish Canyon Tuff age standards at the FRM II reactor in Garching, Germany. External detectors were etched for 18 min in 48% HF at 20°C. Fission tracks were counted at the ISTerre Thermochronology laboratory with an Olympus BX2 microscope at 1250x magnification using the FTstage 4.04 system.

4 Results

4.1 Fluid inclusions

In cleft monazite, primary inclusions occur isolated or form trails of 2-3 inclusions and secondary inclusions are located in healed fracture planes (Figs. 3c and 3d). The size of fluid inclusions ranges from 10x10 µm to less than 4x4 µm for secondary inclusions. In quartz crystals, primary inclusions are also isolated or aligned along trails of 4-5 inclusions parallel to quartz growth faces, whereas secondary inclusions are located on former fissures which crosscut the crystals from rim to core (Figs. 3e and 3f). Quartz populations show euhedral shapes with no evidence of deformation microstructures (Diamond and Tarentola; 2015). The size of primary fluid inclusions in quartz is mostly comparable to that of monazite (~10x10 µm) but can reach ~20x30 µm. Secondary fluid inclusions are smaller than 5x5 µm. All the fluid inclusions investigated are bi-phased, liquid and vapour (L-V type), and homogenize to liquid by heating. No solid phase was observed in the studied fluid inclusions.

Based on the fluid inclusions petrography and microthermometric results, five different sets of fluid inclusions populations were distinguished in monazite and quartz (Fig. 4; Table 1). In cleft monazite (3 crystals), primary fluid inclusions (MnzP*)* have T_h ranging from 283.2 to 345.3°C (N = 10). Three secondary inclusions in monazite crystals (MnzS) were large enough for microthermometric measurements, which give T_h between 203.8 to 241.6°C (N = 3). In cleft quartz (5 crystals), two populations of primary inclusions with different T_h were found: the first (QzP1) corresponds to few inclusions with higher T_h (278.3 to 314.9°C; N = 4) compared to the main second group (QzP2*;* 178.3 to 223.3°C, with a mode around 210°C; N = 46). These two populations are morphologically similar. Secondary inclusions located in quartz samples (QzS*)* give lower T_h (120.6 to 147.7°C; N = 8). Eutectic temperatures were determined between -21.2 and -23°C, which is in good agreement with T_e for H_2O-NaCl and H_2O-NaCl-KCl systems, respectively at -21.2 and -22.9°C (Bodnar, 2003; Hall et al., 1988). For the entire dataset, T_m ice obtained in quartz and monazite crystals overlap within uncertainty: they range from -6.0 to -9.6°C (Fig. 4), which converts to salinities between 9.2 and 13.5 wt.%NaCl equivalent. There is no significant difference in salinities between the 5 fluid inclusion populations, although fluid inclusions trapped at lower temperature have generally lower salinities. Based on similar T_m ice and T_h values (Fig. 4), the first population of quartz inclusions (QzP1) is considered equivalent to primary inclusions in monazite (MnzP*)*, whereas the secondary fluid inclusion population in monazite (MnzS*)* overlap with the main group of primary inclusions in quartz (QzP2). Isochores were calculated using equations of Zhang and Frantz (1987) assuming negligible CO_2 (Poty et al., 1974). MnzP and QzP1 fluid inclusions populations give P-T relationships at 11.0 and 11.8 bar/°C, MnzS and QzP2 populations give 16.3 and 17.0 bar/°C and QzS give 21.4 bar/°C (Fig. 6).

In addition to microthermometric data, fluid composition was measured in primary quartz inclusion (Table 2) to evaluate the trace element concentrations and use the Na/K and Na/Li geothermometers (Can, 2002). Amongst the 47 fluid inclusions analysed in quartz, compositions could be retrieved only for 14 of them, due to low intensity signal and the presence of mineral inclusions. Fluid inclusion compositions were successfully obtained only in the fragments of cm-sized quartz (E2R3a, E2R31a and E2R31b). In these quartz fragments, only fluid inclusions with T_h of the QzP2 group were detected and thus fluid inclusion compositions are attributed to this population (Table 1). In the fluid inclusions, only Na, K, Li, and Sr concentrations are systematically above the detection limit of the LA-ICP-MS measurements. The rare earth

elements (Y, La, Ce, Pr, Nd, Sm), Th, U, As and Ca are generally below the detection limits. The average T_m ice obtained for the QzP_2 fluid inclusions (-7.3°C) was used to calculate the Na concentration of 43300 ppm. This value of 43300 ppm Na was used as an internal standard for the calculation of Li, K and Sr concentrations (Table 2). Although fluid inclusions show different cationic contents, the Na/K ratio in the fluid is equivalent for all the studied crystals (3.7 ± 0.3), confirming that equilibrium between feldspar and fluid is achieved. This Na/K ratio corresponds to T of 280-330°C with most values comprised between 300-320°C (Table 2). Similar temperature interval can be obtained based on the Na/K and Na/Li ratio (Fig. 5), using the geothermomether of Verma and Santoyo (1997). Intersection of this T interval with the QzP2 isochore yields a trapping pressure at 1.5-2.2 kbar (Fig. 6).

4.2 Zircon Fission Tracks

The *R1* sample gave a ZFT central age of 10.3 ± 1 Ma (Fig. 7a), with an age range between 7.2 and 16.7 Ma. The *R2* sample gave a ZFT central age of 16.3 ± 1.9 Ma (Fig. 7b), for an age range between 10.2 and 50.4 Ma. The *R3* sample gave a ZFT central age of 14.3 ± 1.6 Ma (Fig. 7c), with individual grain ages between 5.2 and 20.1 Ma. Normally, the objective is to date at least about 20 grains per sample, which was not possible because of poor sample quality with few zircons available, and many grains with strong U-zoning and inclusions. Therefore only a rather limited number of grains could be analysed per sample, resulting in a relatively high dispersion in the grain age distributions and low $\chi 2$ values. Unfortunately, no significant number of horizontal track lengths could be measured to determine the degree of partial annealing in all three samples. Nonetheless, the fission tracks in sample R1 appeared shorter than in the other two samples. Because of all these limitations the ZFT ages provided here should be viewed with caution. Particularly the two samples collected further away from the cleft may have been affected by partial annealing only. Nonetheless, the observed single grain ages and central ages indicate that these zircons experienced cooling since the mid-Miocene.

5 Discussion

5.1 Hydrothermal activity in the Lauzière Alpine-cleft

Alpine-clefts correspond to fissures that opened up under deformation related to exhumation of the ECM (Mullis et al., 1994; Poty et al., 1974). In Alpine-type clefts, hydrothermal minerals generally precipitate under retrograde metamorphic conditions at temperatures and pressures in the range of 150-450°C and 1.4-3.0 kbar, respectively (Fabre et al., 2002; Mullis et al., 1994; Poty et al., 1974). Cleft mineralogy and geochemistry attest of equilibrium with the neighbouring host-rocks (e.g., Sharp et al., 2005). Furthermore, fluid inclusions (e.g., Mullis et al., 1994) and mineral dating (e.g., Janots et al., 2012) indicate in general episodic crystallisation pulses rather than continuous precipitation due to progressive cooling. In this study, homogenization temperatures and petrographic observations (primary/secondary) of the fluid inclusions indicate three main stages of fluid inclusion entrapment (Fig. 4):

(i) MnzP + QzP1 with highest homogenization temperatures (278-345°C)

(ii) QzP2 + MnzS with intermediate homogenization temperatures (178-242°C)

(iii) QzS with the lowest homogenization temperatures (121-148°C)

All fluid inclusions have equivalent T_m ice (equivalent salinities) suggesting equilibrium between the fluid and the host-rock. Equilibrium is also supported by the consistency of the Na/K ratio measured in the quartz fluid inclusions (QzP2).

Opposite to paragenetic observations that generally suggest a late monazite crystallisation (e.g., Gnos et al., 2015), the petrological observation of quartz lying on monazite and primary fluid inclusions in monazite (MnzP, N = 10; Fig. 4), indicate that monazite precipitates in an early hydrothermal growth stage in the Alpine cleft studied here. This first precipitation stage is independently confirmed by few primary fluid inclusions in quartz (QzP1; N = 4).

The main episode of quartz growth (QzP2; N = 46) is recorded by secondary fluid inclusions in monazite (MnzS; N = 3; Fig. 4), indicating that monazite growth had ceased by then (Fig. 8). This second episode of hydrothermal growth may be caused by oversaturation reached due to cooling, pressure changes, fluid mixing or deformation (e.g. discussion and references in Bergemann et al., 2017). Geothermometry based on the Na/K ratio (and Na/Li) in quartz fluid inclusions (QzP2) indicate that main quartz growth occurred at around 300-320°C (Fig. 5) at P = 1.5-2.2 kbar (Fig. 6). The pressure interval of 1.5-2.2 kbar determined from this group is coherent with previous micrometric studies on fluid inclusions in the ECM (Fabre et al., 2002; Mullis et al., 1994; Poty et al., 1974), and the crustal depth estimated from thermochronological data and assumed geothermal gradients for the Belledonne and surrounding massifs (Fügenschuh and Schmid, 2003; Glotzbach et al., 2011; Seward and Mancktelow, 1994).

Alpine-cleft monazite precipitation temperature can be evaluated from the pressure determined for the main phase of quartz growth (QzP2) assuming no major exhumation occurred in the relatively short duration episode (<3 Myr, see hereafter) between the main phases of monazite (MnzP) and quartz growth (QzP2). Using the pressure interval of 1.5-2.2 kbar determined with QzP2, intersection with the MnzP isochores indicates a maximal T interval of 410-520°C for monazite growth (Fig. 6). This is one of the rare cases where fluid inclusions document a significantly higher fluid temperatures compared to the metamorphic host-rock temperatures (Mullis et al., 1994; Boutoux et al., 2014). This hot fluid circulation would have been overlooked based on quartz fluid inclusions, the number of QzP1 being unrepresentative compared to the QzP2 trapped during the main phase of quartz growth (Fig. 4). To our knowledge, this is one of the first time that fluid inclusions are measured in monazite and it opens a possible avenue to determine early (hot?) stages of hydrothermal precipitation in Alpine clefts. Early precipitation of monazite compared to quartz, may be attributed to its low solubility, but this has to be confirmed in other clefts or for other low-solubility accessory minerals.

5.2 Impact of advective heating on zircon fission track age resetting

Novel ZFT ages obtained in the Lauzière massif (samples R2 and R3) confirm that metamorphic temperatures were high enough to anneal the pre-Alpine ZFT age signature (Yamada et al., 1995). The ZFT dataset indicates that the Lauzière granite cooled below 240-280°C at around 14-16 Ma (Figs. 7 and 8), in good agreement with previous ZFT data in the

Belledonne massif (8-15 Ma; Fügenschuh and Schmid, 2003; Seward and Mancktelow, 1994; Fig. 1b). In the cleft hanging-wall, the rejuvenation of the ZFT age at 10.3 ± 1.0 Ma indicates a resetting of the ZFT geochronological system by advective heating due to the hot hydrothermal fluid penetrating the cleft. This result is similar to previous conclusions reached in the Nojima fault, where modification of the zircon fission track lengths are interpreted as consequences of ancient thermal overprints by heat transfer or dispersion via fluids in the fault zone (Tagami and Murakami, 2007). As in our study, the effect appears extremely local since it is not seen in samples taken at the vicinity of the fault, especially in the footwall (<0.1 m).

It is difficult to quantify the spatial impact of advective heating linked to fluid circulation at the outcrop scale. In the present study, the two samples taken at quite some distance from the cleft (30 m and 100 m) have ZFT ages older than monazite growth in the cleft, indicating no significant resetting by related cleft fluid circulation. However, along the eastern margin of the Lauzière granite, fluid circulation is not restricted to clefts but is evidenced in outcrop by retrogression and growth of mica-like phyllosilicates, as shown in the Mont Blanc massif by Rolland and Rossi (2016), and the formation of centimetric scale veins. It is thus not possible to rule out that the ZFT dataset of the deformed Lauzière granite was not affected by fluid circulation during the deformation phase responsible of the cleft formation or even during an earlier, ductile deformation stage.

5.3 Geodynamic evolution and fluid circulations of the ECM

The ECM are constituted of relatively anhydrous and low-permeability rocks underthrusted at mid-crustal levels during the Oligo-Miocene and then exhumed to form some of the highest Alpine relief today (>4000 m-high peaks). In the Lauzière granite the metamorphic peak, which is not well constrained but estimated at temperatures of <400°C, is assumed to have taken place at around 24-26 Ma (Nziengui, 1993) and more generally at around 24-30 Ma in the ECM. Exhumation in the ECM is normally assumed to start around 18 Ma (Boutoux et al., 2016). Indeed, the new ZFT ages may indicate that the Lauzière granite had cooled below the zircon fission-track closure temperature of about 240-280°C during the mid-Miocene (Fig. 8).

The closure temperature is considered as the temperature at which the fission-track system closes to the loss of fission tracks by annealing and is applicable in case of monotonic cooling (Dodson, 1973). The idea is that no fission-tracks are preserved in the zircon crystals at elevated ambient temperatures, but start to be retained as soon as the crystal cools below the effective closure temperature. The actual value of the closure temperature for the zircon fission-track systems depends on the rate of cooling and the amount of accumulated radiation damage (Bernet, 2009; Brandon et al., 1998 Rahn et al., 2004; Reiners and Brandon, 2006; Tagami, et al., 1998). For natural, radiation-damaged zircons and typical alpine cooling rates of 10-20°C/Myr the closure temperature is about 240 ± 5°C, whereas for zircons with no or very low amounts of radiation damage the closure temperature is about 340 ± 10°C for the same cooling rates (Reiners and Brandon, 2006). The closure temperature should not be confused with the partial annealing zone, which is the temperature range over which fission-tracks are partially but not fully annealed, either during reheating or during very slow cooling through this temaprture range (e.g. Reiners and Brandon, 2006). If heating during the hydrothermal event was sufficiently high to anneal fission tracks

completely in the zircons analysed in this study, then the ZFT cooling ages will reflect post-hydrothermal event cooling mainly related to exhumation, given that the hydrothermal heating event as relatively short-lived and with limited thermal impact of the surrounding country rock on a regional scale. Assuming a general regional geothermal gradient of ~25°C/km and a surface temperature of ~10°C the rocks of the Lauzière granite may have been exhumed from crustal depths of <10 km since 14-16 Ma, (Fig. 8).

In the Alpine cleft, the well-resolved Th-Pb monazite age of 12.4 ± 0.1 Ma (N = 86) indicates for a short-duration growth of the millimetric monazite crystals (Grand'Homme et al., 2016). Combined with the new microthermometric data, the monazite age is interpreted to date the first stage of hydrothermal growth following the fracturation and infiltration of a hot fluid (410-520°C) into the host-rock that had already cooled below 240-280°C (Fig. 8). In other words, there is a 150-250°C temperature difference between the fluid from which monazite precipitates and the fracturing host-rock, in which fluid infiltrates. Assuming an undisturbed crustal geothermal gradient, it implies that the source of the fluid was at least 6-10 km deeper than the host-rock. Based on the structural data of the subvertical cleft (Fig. 2), this age records the circulation of hot fluids through fractures created during a regional phase of dextral transpression in the ECM (Bergemann et al., 2017; Gasquet et al., 2010). Within the Alpine cleft, quartz growth occurred during a second hydrothermal growth stage at T = 300-320°C, comprised between the monazite growth at 12.4 ± 0.1 Ma and the cooling of the cleft hanging wall (sample R3) below 240-280°C, at 10.3 ± 1 Ma (Fig. 8). The difference between these two ages constrains the time range between the infiltration of the hot fluid and cooling down of the cleft wall to temperatures similar to the host-rock, i.e. it limits the duration of advective heating to around 1-3 Myr (Fig. 8), but given the uncertainty of the ZFT age, the heating interval may have been even shorter.

Although the difference between fluid and metamorphic host-rock temperatures (150-250°C) appears unusually high compared to thermal fluid regimes previously documented by fluid inclusions in Alpine-type clefts (Mullis et al., 1994; Poty et al., 1974), deep fluid circulation has been already proposed for some other Alpine-type clefts/veins using isotopic and trace element data (Rossi and Rolland, 2014). This thermal difference attests a fluid channelization along pathways of high permeability for upward flow of deep mid-crustal fluids towards the surface. The required fluid channelization is expected along steeply oriented deformation structures like shear zones, faults and fractures (e.g., Boutoux et al., 2014; Goncalves et al., 2012; Marquer and Burkhard, 1992; Oliot et al., 2014). Considering the position of the Lauzière granite, possible fluid pathways through deeper crustal levels could localize westward along the major Ornon-Roselend fault, or southward along the Fond-de-France fault (Fig. 1b). Based on the mid-crustal depth required for the fluid circulations, it is unclear whether the fluids could be originated from topography-driven circulations of meteoritic water (Diamond et al., 2018; Hofmann et al., 2004; Raimondo et al., 2013), or rather liberated by underthrust rock dehydration due to metamorphic reactions. Dehydration reactions, with a likely origin in the underthrust metasediments, could be a good candidate to account for the episodic, short-duration monazite precipitation observed in Alpine Clefts in the ECM (Grand'Homme et al., 2016). Further relationships between seismicity, fluid circulation and metamorphism could also be here considered (Putnis et al., 2017).

6 Conclusion

This study reveals the potential of investigating fluid inclusions in Alpine-type cleft accessory minerals used more commonly for U-Th-Pb geochronology. Novel fluid inclusion analyses in monazite provide evidence for unusually hot hydrothermal conditions (>410°C), which could have been overlooked based on microthermometric studies of fluid inclusions in quartz only (main growth at 300-320°C). Geochronological constraints on cleft monazite and ZFT, attest that the fluid circulation took place when the host-rock had already cooled below 240-280°C, and heating of the wall-rock lasted <3 Myr. The impact of the hot fluid circulation on estimating cooling rates from thermochronological data in areas affected by hydrothermal fluid flow may be twofold: (1) by causing locally a transient thermal regime and (2) by fully or partially resetting the ZFT thermochronometer. Nonetheless, this effect may possibly only be of importance in the direct vicinity of the areas affected by fluid flow, depending on the size of the fluid conduit, the duration of the fluid flow event and the temperature difference between the hydrothermal fluids and the ambient temperature of the country rock. Advective heating associated with this hot fluid was spatially restricted to the wall-rock of the Alpine-type cleft, although it may be difficult to evaluate the impact of possible pervasive fluid circulation during the faulting of the granite host-rock. A circulating fluid exceeding the cleft host rock temperature by 150-250°C implies fluids over large distance at mid-crustal levels, with a local impact once it migrates through the cleft. Further constraints on the permeability and fluid flux required for this advective heating by hot fluids would require modelling, extensive field mapping of the geological structures (geometry of the vein network and its possible channelization) and geochemical and petrological studies to characterize reactions and mass transfer associated with the fluid circulation.

Author contribution

EJ was the principal investigator of this collaborative project. Most measurements were done by AG'H during his PhD project co-supervised with A-MS-G. Mineral separation, petrography of fluid inclusions and microthermometric measurement were done in collaboration with DG, the LA-ICP-MS measurements on fluid inclusions with MCB. The ZFT analyses were supervised by MB. Sample were collected on the field with EG and RDAG. The timing and conditions of deformation, metamorphism, and fluid circulations in the ECM were thoroughly discussed and controlled with MR.

Acknowledgements

This work was funded by the ANR-12-JS06-0001-01 (MONA) project, and a grant from LabEx OSUG@2020 (Investissements d'avenir – ANR10 LABX56; France). The paper benefited from editorial handling from Bernhard Grasemann and constructive reviews from A. Berger and an anonymous reviewer. Zircon fission track data were obtained thanks to F. Coeur (rock crushing), F. Senebier (mineral separation), M. Balvay (fission track counting) and M. Grosjean (sampling). We thank T. Dumont for fruitful discussions.

References

Austrheim, H. and Griffin, W.: Shear Deformation and Eclogite Formation Within Granulite-Facies Anorthosites of the Bergen Arcs, Western Norway. Chem. Geol. 50, 267–281. https://doi.org/10.1016/0009-2541(85)90124-X, 1985.

Bellanger, M., Augier, R., Bellahsen, N., Jolivet, L., Monié, P., Baudin, T. and Beyssac, O.: Shortening of the European Dauphinois margin (Oisans Massif, Western Alps): New insights from RSCM maximum temperature estimates and 40Ar/39Ar in situ dating. J. Geodyn. 83, 37–64. https://doi.org/10.1016/j.jog.2014.09.004, 2015.

Bergemann, C., Gnos, E., Berger, A., Whitehouse, M., Mullis, J., Wehrens, P., Pettke, T. and Janots, E.: Th-Pb ion probe dating of zoned hydrothermal monazite and its implications for repeated shear zone activity: An example from the Central Alps, Switzerland. Tectonics 36, 2016TC004407. https://doi.org/10.1002/2016TC004407, 2017.

Berger, A., Gnos, E., Janots, E., Whitehouse, M., Soom, M., Frei, R., Waight, T.E.: Dating brittle tectonic movements with cleft monazite: Fluid-rock interaction and formation of REE minerals. Tectonics 32, 1176–1189. https://doi.org/10.1002/tect.20071, 2013.

Bernet, M.: A field-based estimate of the zircon fission-track closure temperature. Chemical Geology 259, 181-189, 2009.

Bodnar, R.J.: Interpretation of Data from Aqueous-Electrolyte Fluid Inclusion. In:(Samson, I., Alderton, A., and Marshall, D. Eds.), *Fluid Inclusions : Analysis and Interpretation*. Mineralogical Association of Canada, 2003.

Boutoux, A., Verlaguet, A., Bellahsen, N., Lacombe, O., Villemant, B., Caron, B., Martin, E., Assayag, N. and Cartigny, P.: Fluid systems above basement shear zones during inversion of pre-orogenic sedimentary basins (External Crystalline Massifs, Western Alps). Lithos 206–207, 435–453. https://doi.org/10.1016/j.lithos.2014.07.005, 2014.

Boutoux, A., Bellahsen, N., Nanni, U., Pik, R., Verlaguet, A., Rolland, Y. and Lacombe, O.: Thermal and structural evolution of the external Western Alps: Insights from (U–Th–Sm)/He thermochronology and RSCM thermometry in the Aiguilles Rouges/Mont Blanc massifs. Tectonophysics 683, 109–123. https://doi.org/10.1016/j.tecto.2016.06.010, 2016.

Brandon, M.T., Roden-Tice, M.K., and Garver, J.I., Late Cenozoic exhumation of the Cascadia accretionary wedge in the Olympic Mountains, Northwest Washington State. Geol. Soc. Am. Bull. 110:985–1009, 1998.

Can, I.: A new improved Na/K geothermometer by artificial neural networks. Geothermics 31, 751–760. https://doi.org/10.1016/S0375-6505(02)00044-5, 2002.

Cenki-Tok, B., Darling, J.R., Rolland, Y., Dhuime, B. and Storey, C.D.: Direct dating of mid-crustal shear zones with synkinematic allanite: new in situ U-Th-Pb geochronological approaches applied to the Mont Blanc massif. Terra Nova 26, 29–37. https://doi.org/10.1111/ter.12066, 2014.

Debon, F., Guerrot, C., Menot, R.P., Vivier, G. and Cocherie, A.: Late Variscan granites of the Belledonne massif (French western Alps): an early Visean magnesian plutonism. Schweiz. Mineral. Petrogr. Mitteilungen 78, 67–85, 1998.

Derry, L.A., Evans, M.J., Darling, R. and France-Lanord, C.: Hydrothermal heat flow near the Main Central Thrust, central Nepal Himalaya. Earth Planet. Sci. Lett. 286, 101–109. https://doi.org/10.1016/j.epsl.2009.06.036, 2009.

Diamond, L.-W. and Tarantola, A.: Interpretation of fluid inclusions in quartz deformed by weak ductile shearing: Reconstruction of differential stress magnitudes and pre-deformation fluid propoerties. Earth Planet. Sci. Lett. 417, 107–

119. https://doi.org/10.1016/j.epsl.2015.02.019, 2015.

Diamond, L.W., Wanner, C. and Waber, H.N.: Penetration depth of meteoric water in orogenic geothermal systems. Geology. https://doi.org/10.1130/G45394.1, 2018

Dodson, M.H.: Closure temperature in cooling geochronological and petrological systems, Contrib. Mineral. Petrol. 40, 259–74, 1973.

Dumont, T., Champagnac, J.-D., Crouzet, C. and Rochat, P.: Multistage shortening in the Dauphiné zone (French Alps): the record of Alpine collision and implications for pre-Alpine restoration. Swiss J. Geosci. 101, 89–110. https://doi.org/10.1007/s00015-008-1280-2, 2008.

Engi, M., Lanari, P. and Kohn, M.J.: Significant Ages—An Introduction to Petrochronology. Rev. Mineral. Geochem. 83, 1–12. https://doi.org/10.2138/rmg.2017.83.1, 2017.

Fabre, C., Boiron, M.-C., Dubessy, J., Cathelineau, M. and Banks, D.A.: Palaeofluid chemistry of a single fluid event: a bulk and in-situ multi-technique analysis (LIBS, Raman Spectroscopy) of an Alpine fluid (Mont-Blanc). Chem. Geol. 182, 249–264. https://doi.org/10.1016/S0009-2541(01)00293-5, 2002.

Fügenschuh, B. and Schmid, S.M. Late stages of deformation and exhumation of an orogen constrained by fission-track data: A case study in the Western Alps. GSA Bull. 115, 1425–1440. https://doi.org/10.1130/B25092.1, 2003.

Gasquet, D., Bertrand, J.-M., Paquette, J.-L., Lehmann, J., Ratzov, G., Guedes, R.D.A., Tiepolo, M., Boullier, A.-M., Scaillet, S. and Nomade, S.: Miocene to Messinian deformation and hydrothermal activity in a pre-Alpine basement massif of the French western Alps: new U-Th-Pb and argon ages from the Lauziere massif. Bull. Soc. Geol. Fr. 181, 227–241. https://doi.org/10.2113/gssgfbull.181.3.227, 2010.

Glotzbach, C., van der Beek, P.A. and Spiegel, C.: Episodic exhumation and relief growth in the Mont Blanc massif, Western Alps from numerical modelling of thermochronology data. Earth Planet. Sci. Lett. 304, 417–430. https://doi.org/10.1016/j.epsl.2011.02.020, 2011.

Gnos, E., Janots, E., Berger, A., Whitehouse, M., Walter, F., Pettke, T. and Bergemann, C.: Age of cleft monazites in the eastern Tauern Window: constraints on crystallization conditions of hydrothermal monazite. Swiss J. Geosci. 108, 55–74. https://doi.org/10.1007/s00015-015-0178-z, 2015.

Goncalves, P., Oliot, E., Marquer, D. and Connolly, J. a. D.: Role of chemical processes on shear zone formation: an example from the Grimsel metagranodiorite (Aar massif, Central Alps). J. Metamorph. Geol. 30, 703–722. https://doi.org/10.1111/j.1525-1314.2012.00991.x, 2012.

Grand'Homme, A., Janots, E., Bosse, V., Seydoux-Guillaume, A.M. and Guedes, R.D.A.: Interpretation of U-Th-Pb in-situ ages of hydrothermal monazite-(Ce) and xenotime-(Y): evidence from a large-scale regional study in clefts from the western alps. Mineral. Petrol. 1–21. https://doi.org/10.1007/s00710-016-0451-5, 2016.

Hall, D.L., Sterner, S.M. and Bodnar, R.J.: Freezing point depression of NaCl-K-Cl-H_2O solutions. Economic Geology 83, 197-202, 1988.

Hofmann, B.A., Helfer, M., Diamond, L.W., Villa, I.M., Frei, R. and Eikenberg, J.: Topography-driven hydrothermal breccia

mineralization of Pliocene age at Grimsel Pass, Aar massif, Central Swiss Alps. Schweiz. Mineral. Petrogr. Mitteilungen 84, 271–302, 2004.

Janots, E., Berger, A., Gnos, E., Whitehouse, M., Lewin, E. and Pettke, T.: Constraints on fluid evolution during metamorphism from U–Th–Pb systematics in Alpine hydrothermal monazite. Chem. Geol. 326–327, 61–71. https://doi.org/10.1016/j.chemgeo.2012.07.014, 2012.

Leisen, M., Boiron, M.C., Richard, A. and Dubessy, J.: Determination of Cl and Br concentrations in individual fluid inclusions by combining microthermometry and LA-ICPMS analysis: Implication for the origin of salinity in crustal fluids. Chem. Geol. 330-331, 197-206. https://doi.org/10.1016/j.chemgeo.2012.09.003, 2012.

Leloup, P.H., Arnaud, N., Sobel, E.R. and Lacassin, R.: Alpine thermal and structural evolution of the highest external crystalline massif: The Mont Blanc. Tectonics 24, TC4002. https://doi.org/10.1029/2004TC001676, 2005.

Marquer, D. and Burkhard, M.: Fluid circulation, progressive deformation and mass-transfer processes in the upper crust: the example of basement-cover relationships in the External Crystalline Massifs, Switzerland. J. Struct. Geol. , 1992.

Moëlo, Y., Palvadeau, P., Meisser, N. and Meerschaut, A.: Structure cristalline d'une ménéghinite naturelle pauvre en cuivre, Cu0,58Pb12,72(Sb7,04Bi0,24)S24. Comptes Rendus Geosci. 334, 529–536. https://doi.org/10.1016/S1631-0713(02)01792-3, 2002.

Mullis, J., Dubessy, J., Poty, B. and O'Neil, J.: Fluid regimes during late stages of a continental collision: Physical, chemical, and stable isotope measurements of fluid inclusions in fissure quartz from a geotraverse through the Central Alps, Switzerland. Geochim. Cosmochim. Acta 58, 2239–2267. https://doi.org/10.1016/0016-7037(94)90008-6, 1994.

Nziengui, J.J.: Excès d'argon radiogénique dans le quartz des fissures tectoniques: implications pour la datation des séries méthamorphiques. L'exemple de la coupe de la Romanche, Alpes Occidentales françaises (Thèse 3ème cycle). Université Joseph Fourier, Grenoble, France, 209 p., 1993.

Oliot, E., Goncalves, P., Schulmann, K., Marquer, D. and Lexa, O.: Mid-crustal shear zone formation in granitic rocks: Constraints from quantitative textural and crystallographic preferred orientations analyses. Tectonophysics 612–613, 63–80. https://doi.org/10.1016/j.tecto.2013.11.032, 2014.

Poty, B.P., Stalder, H.A. and Weisbrod, A.M.: Fluid inclusions studies in quartz from fissures of Western and Central Alps. Schweiz. Mineral. Petrogr. Mitteilungen 717–752, 1974.

Putnis, A. and Austrheim, H.: Fluid-induced processes: metasomatism and metamorphism. Geofluids 10, 254–269. https://doi.org/10.1111/j.1468-8123.2010.00285.x, 2010.

Putnis, A., Jamtveit, B. and Austrheim, H.: Metamorphic Processes and Seismicity: the Bergen Arcs as a Natural Laboratory. J. Petrol. 58, 1871–1898. https://doi.org/10.1093/petrology/egx076, 2017.

Rahn, M.K., Brandon, M.T., Batt, G.E., and Garver, J.I.: A zero-damage model for fission track annealing in zircon. Am. Mineral. 89, 473–484, 2004.

Raimondo, T., Clark, C., Hand, M., Cliff, J. and Anczkiewicz, R.: A simple mechanism for mid-crustal shear zones to record surface-derived fluid signatures. Geology 41, 711–714. https://doi.org/10.1130/G34043.1, 2013.

Reiners, P.W. and Brandon, M.T.: Using thermochronology to understand orogenic erosion. Annu. Rev. Earth Planet. Sci. 34, 419–466, 2006.

Roedder, E. *Fluid Inclusions*. Mineralogical Society of America, 646 p., 1984.

Rolland, Y., Cox, S., Boullier, A.-M., Pennacchioni, G. and Mancktelow, N.: Rare earth and trace element mobility in mid-crustal shear zones: insights from the Mont Blanc Massif (Western Alps). Earth Planet. Sci. Lett. 214, 203–219. https://doi.org/10.1016/S0012-821X(03)00372-8, 2003.

Rolland, Y. and Rossi, M.: Two-stage fluid flow and element transfers in shear zones during collision burial-exhumation cycle: Insights from the Mont Blanc Crystalline Massif (Western Alps). J. Geodyn. 101, 88–108. https://doi.org/10.1016/j.jog.2016.03.016, 2016.

Rosenberg, C.L. and Berger, A.: On the causes and modes of exhumation and lateral growth of the Alps. Tectonics 28, TC6001. https://doi.org/10.1029/2008TC002442, 2009.

Rossi, M. and Rolland, Y.: Stable isotope and Ar/Ar evidence of prolonged multiscale fluid flow during exhumation of orogenic crust: Example from the Mont Blanc and Aar Massifs (NW Alps). Tectonics 33, 1681–1709. https://doi.org/10.1002/2013TC003438, 2014.

Rossi, M., Rolland, Y. and Cox, S.F.: Geochemical variations and element transfer during shear-zone development and related episyenites at middle crust depths: insights from the Mont Blanc granite (French-Italian Alps). High-Strain Zones Struct. Phys. Prop. 245, 373–396. https://doi.org/10.1144/GSL.SP.2005.245.01.18, 2005.

Seward, D. and Mancktelow, N.: Neogene Kinematics of the Central and Western Alps - Evidence from Fission-Track Dating. Geology 22, 803–806. https://doi.org/10.1130/0091-7613(1994)022<0803:NKOTCA>2.3.CO;2, 1994.

Shepherd, T.J., Rankin, A.H. and Alderton, D.H.M.: A Practical Guide to Fluid Inclusion Studies. 293pp., 1985.

Sharp, Z.D., Masson, H. and Lucchini, R.: Stable isotope geochemistry and formation mechanisms of quartz veins; extreme paleoaltitudes of the Central Alps in the Neogene. Am. J. Sci. 305, 187–219. https://doi.org/10.2475/ajs.305.3.187, 2005.

Simon-Labric, T., Rolland, Y., Dumont, T., Heymes, T., Authemayou, C., Corsini, M. and Fornari, M.: 40Ar/ 39Ar dating of Penninic Front tectonic displacement (W Alps) during the Lower Oligocene (31–34 Ma). Terra Nova 21, 127–136. https://doi.org/10.1111/j.1365-3121.2009.00865.x, 2009.

Tagami, T., and Murakami, M.: Probing fault zone heterogeneity on the Nojima fault: Constraints from zircon fission-track analysis of borehole samples. Tectonophysics 443, 139–152, 2007.

Tagami, T., Galbraith, R.F., Yamada, R., and Laslett, G.M.: Revised annealing kinetics of fission tracks in zircon and geologic implications. In Advances in Fission-Track Geochronology, ed. P van den Haute, F De Corte, pp. 99–112. Dordrecht: Kluwer Acad. Publ., 1998.

Verma, S.P. and Santoyo, E.: New improved equations for NaK, NaLi and SiO2 geothermometers by outlier detection and rejection. J. Volcanol. Geotherm. Res. 79, 9–23. https://doi.org/10.1016/S0377-0273(97)00024-3, 1997.

Whipp, D.M. and Ehlers, T.A. Influence of groundwater flow on thermochronometer-derived exhumation rates in the central

Nepalese Himalaya. Geology 35, 851–854. https://doi.org/10.1130/G23788A.1, 2007.

Yamada, R., Tagami, T., Nishimura, S. and Ito, H.: Annealing kinetics of fission tracks in zircon: an experimental study. Chem. Geol. 122, 249–258. https://doi.org/10.1016/0009-2541(95)00006-8, 1995.

Zhang, Y.G. and Frantz, J.D.: Determination of the homogenization temperatures and densities of supercritical fluids in the system NaCl-KCl-$CaCl_2$-H_2O using synthetic fluid inclusions. Chem. Geol. 64, 335-350, 1987.

Figures

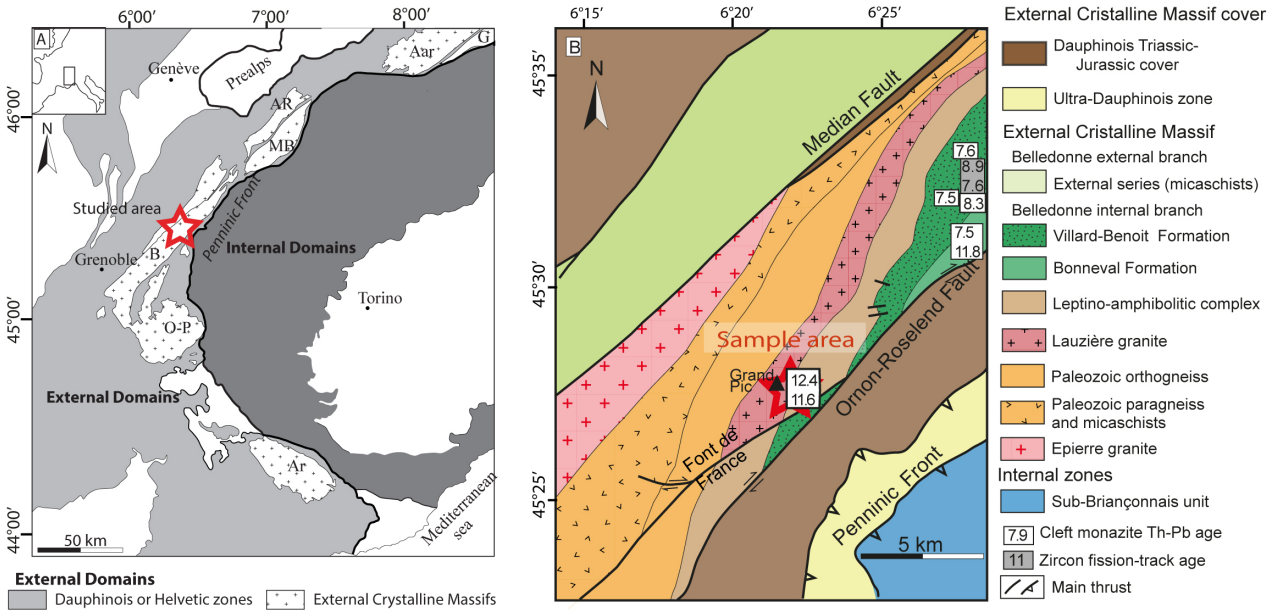

Figure 1: Simplified geological maps showing the location of the investigated area (red star). (A) Western Alps with the location of the External Crystalline Massifs: Aar; G: Gotthard; AR: Aiguilles Rouges; MB: Mont Blanc; B: Belledonne; P: Pelvoux; O: Oisans; Ar: Argentera. (B) Main geological units of the Lauzière massif. Grey rectangles are zircon fission-track central ages (Fügenschuh and Schmid, 2003), white rectangles are cleft monazite Th-Pb ages (Gasquet et al., 2010; Grand'Homme et al., 2016).

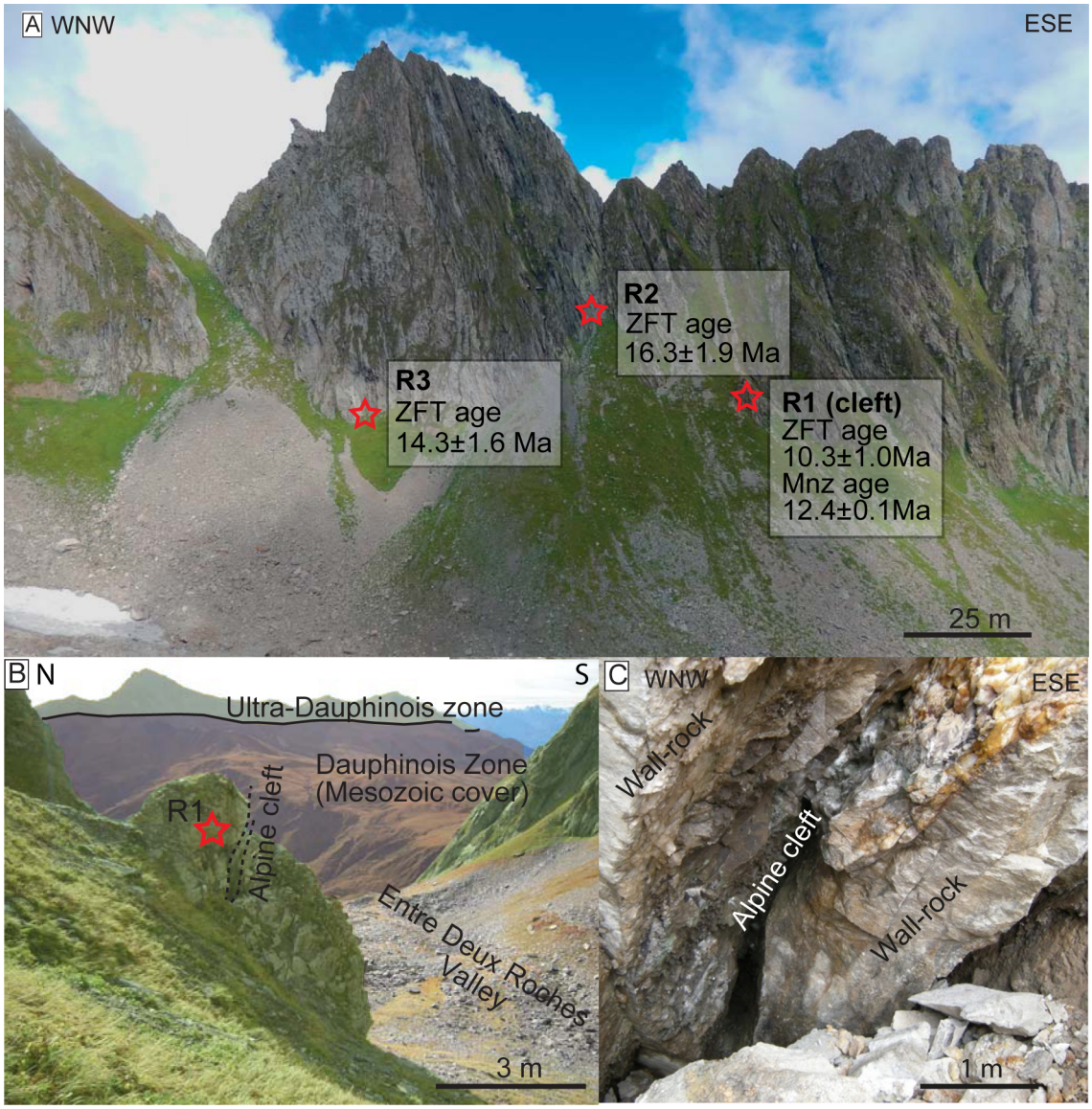

Figure 2: Photographs of the investigated outcrop. (A) *Entre Deux Roches* profile with location and ages of the investigated samples represented by red stars: R1 corresponds to the position of the cleft and its wall-rock (45°28'52.90"N; 6°23'6.18"E), R2 and R3 were taken at 30 m and 100 m away from the cleft. (B) Alpine-type cleft location with location of the R1 sample taken in the wall-rock of the cleft. The N110 oriented subvertical vein is perpendicular to the main N010-020 mylonitic subvertical foliation (C) Detail of the Alpine-type cleft showing the hydrothermal crystals and the leached wall-rock.

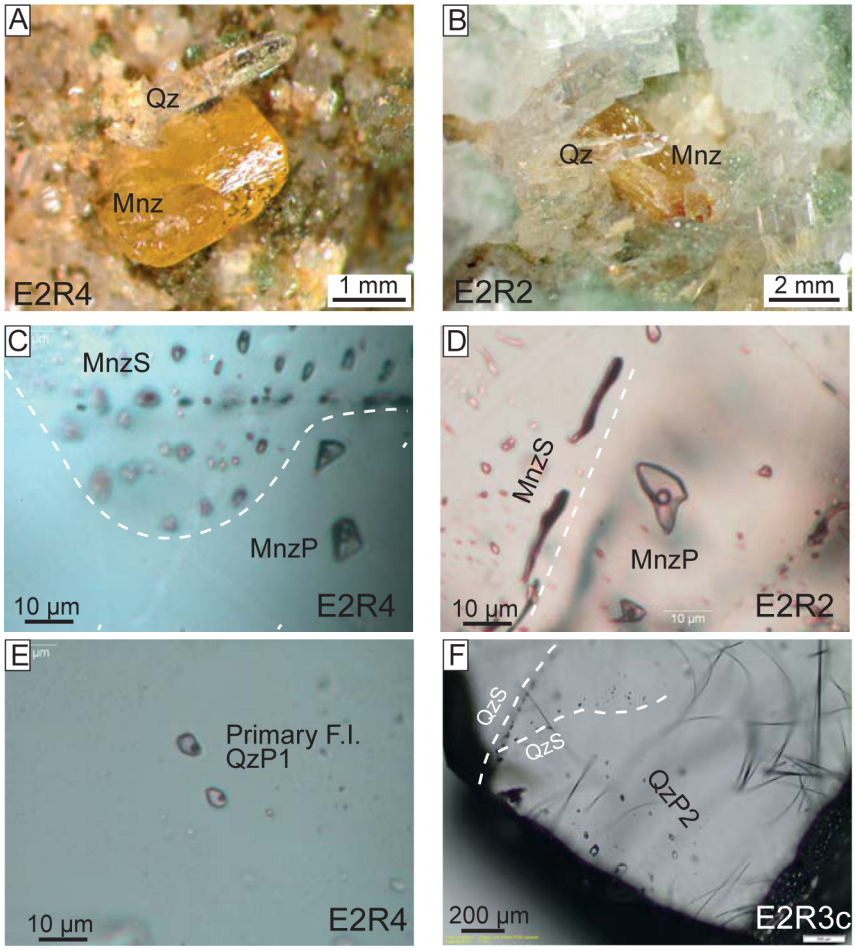

Figure 3: Photographs and microphotographs (C-D-E-F) of cleft quartz (Qz) and monazite (Mnz) crystals and their fluid inclusions. (A) and (B): contiguous quartz and monazite crystals used for fluid inclusion microanalyses (samples E2R4 et E2R2, respectively). (C) and (D): fluid inclusions in monazite: note that primary fluid inclusions (MnzP; around 10 µm) are found in limpid domains whereas secondary fluid inclusions (MnzS; <5 µm) form trails; (E) and (F) Fluid inclusions in quartz: the two populations of primary inclusions (QzP1 and QzP2) have similar morphologies (euhedral with typical size of 10 µm) and are found in limpid quartz domains while the secondary fluid inclusions are smaller and found aligned along trails. Black mineral fibers are meneghinite ($Pb_{13}CuSb_7S_{24}$; Moëlo et al., 2002)

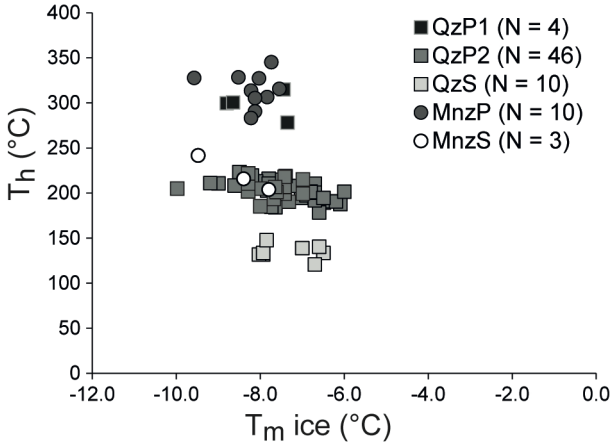

Figure 4: T_h vs. T_m ice diagram of the fluid inclusions data. QzP1: population 1 of primary fluid inclusions in quartz; QzP2: population 2 of primary fluid inclusions in quartz; QzS: secondary fluid inclusions in quartz; MnzP: primary fluid inclusions in monazite; MnzS: secondary fluid inclusions in monazite

5

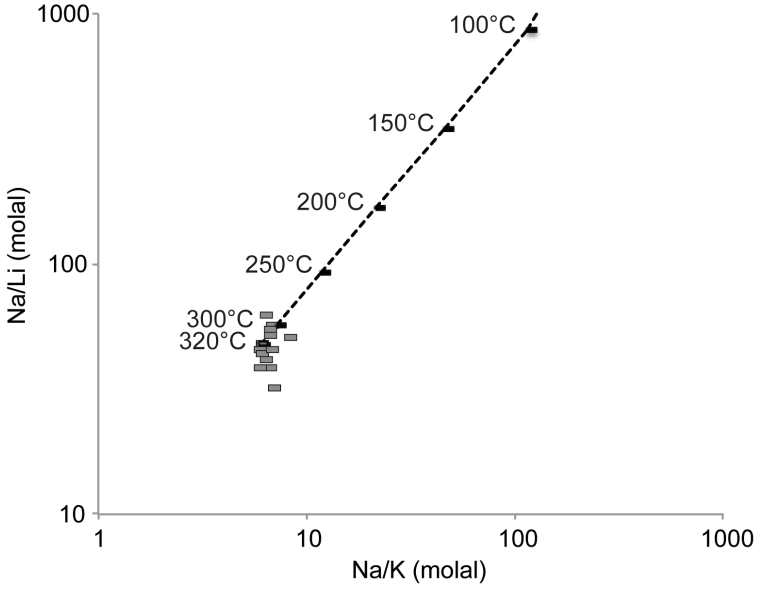

Figure 5: Na/K versus Na/Li ratio measured in quartz fluid inclusions (QzP2). The dash line corresponds to geothermometry calibrations from Verma and Santoyo (1997). The dataset indicates a temperature growth at 300-320°C.

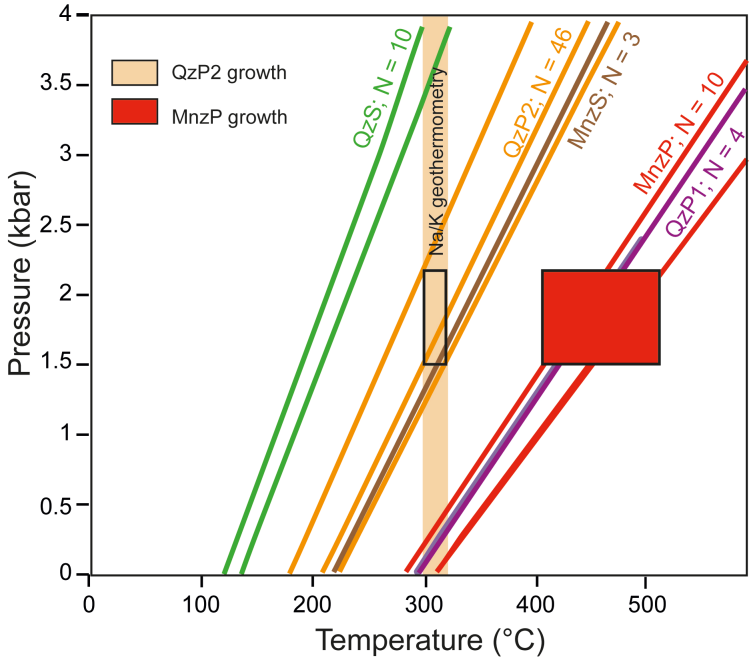

Figure 6: Geothermobarometric results obtained for fluid inclusions of the Alpine-cleft. Mean isochoric P-T relationships calculated from microthermometric measurements of fluid inclusions in monazite and quartz showing three main stages of growth. Fluid inclusion populations and number of analyses are indicated. P-T estimation for the main episode of quartz growth (QzP2) is obtained by the intersection of the T interval determined by the Na/K geothermometer (300-320°C) with the QzP2 isochore. It gives a pressure estimates of 1.5-2.2 kbar for the main phase of quartz growth, that was used to determine the maximal T range (410-520°C) for monazite (MnzP) growth.

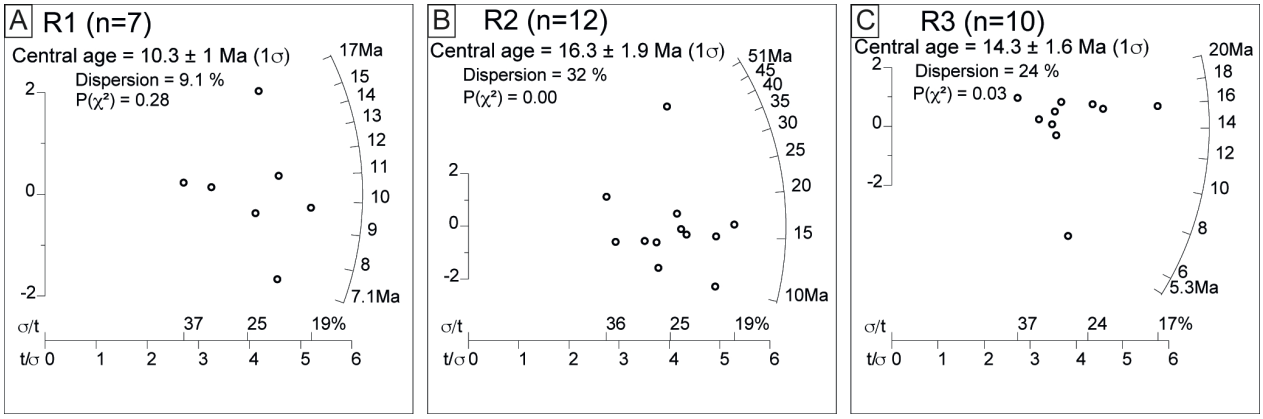

Figure 7: Radial plots of zircon ages in the granite host-rock. (A) *R1* sample (cleft hanging-wall). (B) *R2* sample (~30 m from the cleft). (C) *R3* sample (~100 m from the cleft)

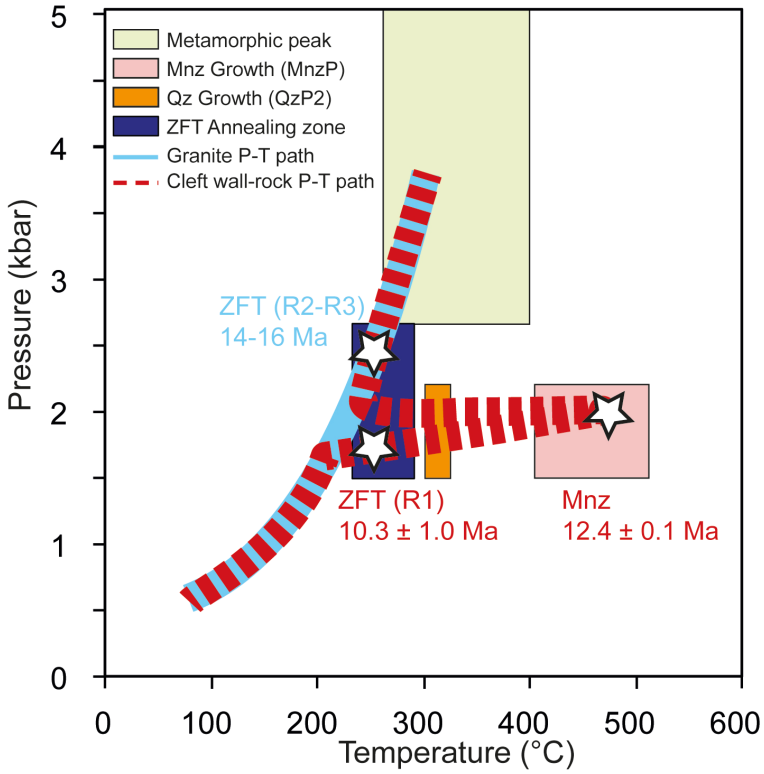

Figure 8: Pressure-temperature (P-T) path for the Lauzière granite host-rock and in the hanging wall of the Alpine-type cleft. Metamorphic peak conditions are not well constrained in the Lauzière massif, and are based on a compilation of metamorphic and geochronological data in the external massifs from the Western Alps (Rolland et al., 2003; Rossi et al., 2005; Simon-Labric et al., 2009; Bellanger et al., 2015). Geochronological constrains provided in this study are represented by stars. The zircon fission track (ZFT) thermochronometer fixes the cooling of the granite (R2-R3) and the cleft (R1) below 240-280°C. Microthermometric and geochronological results on monazite (Mnz) are assumed to represent the onset of hydrothermal activity (red box); while the main hydrothermal growth phase is based on microthermometric study of the fluid inclusions in quartz (QzP2).

Table 1: Microthermometric analyses of fluid inclusions in monazite (Mnz) and quartz (Qz)

Sample	Mineral	Type	T_e (°C)	T_m ice (°C)	T_h (°C)	Population
E2R1	Qz	Primary	-21.3	-7.8	210.4	QzP2
E2R1	Qz	Secondary	-21.3	-6.7	120.6	QzS
E2R1	Qz	Primary	-	-8.2	219.3	QzP2
E2R2	Mnz	Primary	-	-7.5	315.5	MnzP
E2R2	Mnz	Primary	-	-8.0	327.3	MnzP
E2R2	Mnz	Primary	-22.9	-7.7	345.3	MnzP
E2R2	Mnz	Primary	-23.1	-9.6	327.6	MnzP
E2R2	Mnz	Secondary	-	-9.5	241.6	MnzS
E2R2	Mnz	Primary	-22.8	-8.5	328.4	MnzP
E2R2	Qz	Primary	-22.4	-7.6	184.3	QzP2
E2R2	Qz	Primary	-	-7.4	314.9	QzP1
E2R2	Qz	Primary	-	-8.6	208.2	QzP2
E2R2	Qz	Primary	-23.0	-7.7	184.6	QzP2
E2R2	Qz	Primary	-22.7	-7.8	202.8	QzP2
E2R2	Qz	Primary	-	-6.1	187.7	QzP2
E2R2	Qz	Primary	-	-6.5	189.6	QzP2
E2R2	Qz	Primary	-	-6.3	190.8	QzP2
E2R2	Qz	Primary	-	-7.0	194.5	QzP2
E2R2	Qz	Primary	-	-7.4	278.3	QzP1
E2R3a	Mnz	Secondary	-21.2	-8.4	215.7	MnzS
E2R3a	Mnz	Secondary	-	-7.8	203.8	MnzS
E2R3a	Qz	Primary	-	-6.7	200.4	QzP2
E2R3a	Qz	Primary	-	-6.2	190.5	QzP2
E2R3a	Qz	Primary	-21.3	-7.8	215.8	QzP2
E2R3a	Qz	Primary	-	-8.1	212.9	QzP2
E2R3a	Qz	Secondary	-21.3	-6.5	133.5	QzS
E2R3a	Qz	Primary	-	-7.4	218.6	QzP2
E2R3a	Qz	Secondary	-	-6.6	140.4	QzS
E2R3a	Qz	Primary	-	-6.8	201.4	QzP2
E2R3b	Qz	Primary	-21.3	-6.7	200.2	QzP2
E2R3b	Qz	Primary	-21.3	-6.9	197.5	QzP2
E2R3b	Qz	Primary	-	-7.3	207.9	QzP2
E2R3b	Qz	Primary	-21.3	-6.6	178.3	QzP2
E2R3b	Qz	Primary	-22.8	-7.7	214.7	QzP2
E2R3b	Qz	Primary	-	-6.7	210.3	QzP2
E2R3b	Qz	Primary	-	-6.7	191.9	QzP2
E2R3c	Qz	Primary	-21.2	-6.8	201.6	QzP2
E2R3c	Qz	Primary	-	-6.8	201.0	QzP2
E2R3c	Qz	Secondary	-21.2	-7.0	138.9	QzS
E2R3c	Qz	Primary	-21.0	-6.5	194.5	QzP2
E2R3c	Qz	Primary	-	-8.5	223.3	QzP2

E2R3c	Qz	Primary	-	-6.0	201.4	QzP2
E2R4	Mnz	Primary	-	-7.8	306.6	MnzP
E2R4	Mnz	Primary	-	-8.2	313.5	MnzP
E2R4	Mnz	Primary	-	-8.1	305.3	MnzP
E2R4	Mnz	Primary	-	-8.1	290.5	MnzP
E2R4	Mnz	Primary	-	-8.2	283.2	MnzP
E2R4	Qz	Primary	-	-8.8	299.6	QzP1
E2R4	Qz	Primary	-22.8	-9.0	210.7	QzP2
E2R4	Qz	Primary	-	-9.2	211.0	QzP2
E2R4	Qz	Primary	-22.9	-7.5	210.0	QzP2
E2R4	Qz	Primary	-	-7.7	210.3	QzP2
E2R4	Qz	Secondary	-	-7.9	131.6	QzS
E2R4	Qz	Secondary	-	-8.0	131.6	QzS
E2R4	Qz	Secondary	-	-7.9	133.5	QzS
E2R4	Qz	Secondary	-	-7.9	147.7	QzS
E2R31a	Qz	Primary	-	-7.3	213.1	QzP2
E2R31a	Qz	Primary	-	-7.3	199.9	QzP2
E2R31a	Qz	Primary	-	-7.5	202.0	QzP2
E2R31a	Qz	Primary	-	-7.5	193.9	QzP2
E2R31a	Qz	Primary	-	-6.9	203.5	QzP2
E2R31a	Qz	Primary	-	-8.2	217.4	QzP2
E2R31a	Qz	Primary	-	-8.2	200.9	QzP2
E2R31a	Qz	Primary	-	-7.9	186.3	QzP2
E2R31a	Qz	Primary	-	-7.2	190.9	QzP2
E2R31b	Qz	Primary	-	-9.8	201.1	QzP2
E2R31b	Qz	Primary	-	-7.9	200.9	QzP2
E2R31b	Qz	Primary	-	-6.9	199.2	QzP2
E2R31b	Qz	Primary	-	-7.0	200.4	QzP2
E2R31b	Qz	Primary	-	-6.9	211.0	QzP2

Table 2: Compositional data of fluid inclusions (QzP2) obtained from LA-ICPMS measurements with Na fixed at 43300 ppm for all inclusions. Temperatures (T) were estimated using the Na/K geothermometers of Can (2002).

Sample	Element concentrations (ppm)			T(°C)
	Li (7)	K (39)	Sr (88)	
DL	*26*	*180*	*1*	
E2R3A	210	11800	430	320
E2R3A	340	11400	530	310
E2R3B	250	11300	470	310
ER31A	290	12000	350	320
ER31A	290	12700	690	330
ER31A	230	11200	370	310
ER31A	320	12000	1440	320
ER31A	410	10900	1050	310
ER31A	300	12500	1090	320
E2R31B	290	11200	740	310
E2R31B	240	11500	770	310
E2R31B	270	12400	850	320
E2R31B	340	12800	1080	330
E2R31B	260	9200	690	280

DL: detection limit